INTERNATIONAL JOURNAL FOR NUMERICAL METHODS IN FLUIDS
Int. J. Numer. Meth. Fluids 2005; **49**:439–464
Published online 8 June 2005 in Wiley InterScience (www.interscience.wiley.com). DOI: 10.1002/fld.1007

Numerical simulation of two-dimensional laminar incompressible offset jet flows

P. Rajesh Kanna[‡,§] and Manab Kumar Das[*,†,¶]

Department of Mechanical Engineering, Indian Institute of Technology Guwahati, North Guwahati, Guwahati 781039, Assam, India

SUMMARY

Two-dimensional transient laminar incompressible offset jet is simulated numerically to gain insight into convective recirculation and flow processes induced by an offset jet. The behaviour of the jet with respect to offset ratio (OR) and Reynolds number (Re) are described in detail. The transient development of the velocity is simulated for various regions: recirculation, impingement and wall jet development. It is found that the reattachment length is dependent on both Re and OR for the range considered. Simulations are made to show the effect of entrainment on recirculation eddy. A detailed study of u velocity decay is reported. The decay rate of horizontal velocity component (u) is linear in impingement region. It is found that at high OR, velocity decay depends on Re only. Velocity profile in the wall jet region shows good agreement with experimental as well as similarity solutions. It is found that the effect of Re and OR are significant to bottom wall vorticity up to impingement region. Far downstream bottom wall vorticity is independent of OR. Copyright © 2005 John Wiley & Sons, Ltd.

KEY WORDS: offset jet; recirculation; velocity decay

1. INTRODUCTION

Depending upon the distance of the confining boundaries from the discharge, a jet can be analysed as a free jet or a bounded one. If the boundaries (parallel to inlet axis) are sufficiently away from the origin of the jet, the flow is termed as a free jet. However, a bounded jet will occur when it interacts with a parallel wall. Bounded jet flows occur in many engineering

*Correspondence to: M. K. Das, Department of Mechanical Engineering, Indian Institute of Technology Guwahati, North Guwahati, Guwahati 781039, Assam, India.
†E-mail: manab@iitg.ernet.in
‡E-mail: rajeshk@iitg.ernet.in; rajeshkanna_p75@yahoo.com
§Research Scholar.
¶Associate Professor.

Received 2 December 2004
Revised 14 April 2005
Accepted 27 April 2005

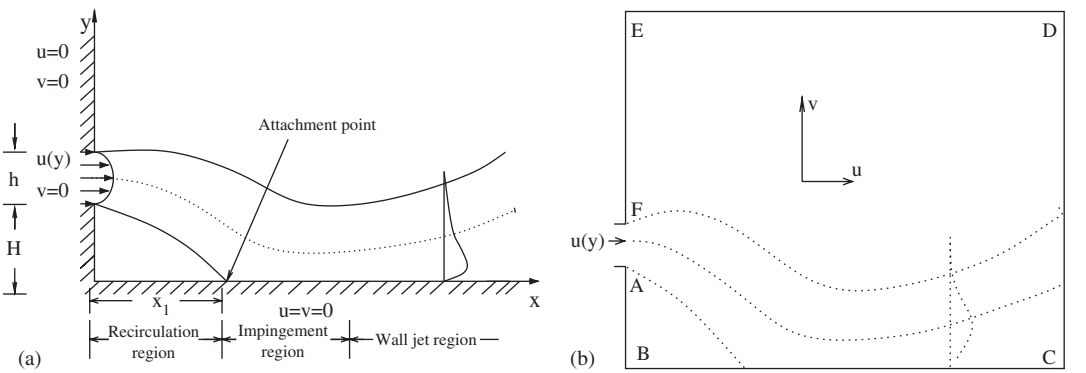

Figure 1. Schematic diagram and boundary conditions of an offset jet problem: (a) schematic of the problem; and (b) computational domain.

applications such as environmental discharges, heat exchangers, fluid injection systems, cooling of combustion chamber wall in a gas turbine, automobile demister and others. Bounded jets can be classified into three types: (a) impinging jet aimed toward the boundary; (b) wall jet where fluid is discharged at the boundary; and (c) offset jet from a vertical wall of a stagnant pool issuing parallel to a horizontal solid wall.

The flow emanating from a two-dimensional (2D) offset jet is shown in Figure 1(a) where the main features and regions of interest are depicted. Fluid is discharged from a slot in a vertical wall into the ambient near a horizontal solid boundary parallel to the inlet jet direction. Due to the entrainment of fluid between the jet and the bottom plate, there is a reduction of pressure in this region forcing the jet to deflect towards the boundary and eventually attach with it. This is called Coanda effect [1]. The offset jet flow features are different in various regions. In the near field within a very short distance from the point of discharge, the jet flow is dominated by momentum and has the properties of a free jet. Attachment occurs when the jet is deflected towards an adjacent solid wall and tends to flow along the boundary. In the region around the attachment point, that is, the impingement region and part of the recirculation region, the jet can be partly characterized as an impingement jet. The offset jet becomes a wall jet in the far field. Other factors like free-stream velocity, ambient stratification, buoyancy (density difference), discharge orientation, etc. further complicate the jet-boundary interaction and the behaviour of an offset jet.

The understanding of the flow behaviour of an offset jet is important in engineering practices. If attachment is not desired for more mixing, knowledge of calculation and design is required to prevent it. For a case where attachment is desirable, study of the involved variables is required so that a precise location of the attachment point and the containment of the flow can be established.

In the present work, the flow features and entrainment characteristics of offset jets are investigated. Analytical solutions of the wall jet are available, based on the self-similarity solution of the velocity field by Glauert [2] and Schlichting and Gersten [3]. However, these solutions are valid only far away from the jet inlet, and in most applications, the near field development holds the key to important features of the jet flow. Therefore, the

near field development of a wall jet has been the subject of a lot of research in recent years.

The mean velocity profile in the longitudinal and transverse directions and the similarity nature are experimentally observed by Chandrasekhara Swamy and Bandyopadhyay [4] for a three-dimensional (3D) wall jet. The wall jet was generated by tangential flow of air from one-half of a round nozzle on to a smooth at plate in a stagnant surrounding. Though the work was carried out for a 3D case, the observations presented are relevant to the present work. Cohen *et al.* [5] did work on the transition of wall jets subjected to blowing and suction. The purpose was to find out the effect of suction and blowing as the alternative controlling method for 2D incompressible wall jet instead of heating and cooling process. Amitay and Cohen [6] have reported the effects of wall blowing and suction on the stability characteristics of a laminar incompressible 2D plane wall jet. They have reported that blowing and suction have the opposite effect on the viscous and inviscid instability modes. Quintana *et al.* [7] experimentally investigated the mean and fluctuating characteristics of a plane unsteady laminar wall jet for constant wall temperature. Seidel [8] has done numerical work to find out the effect of high amplitude forcing on laminar and turbulent wall jet over a heated flat plate. Seidel has used DNS for laminar case and RANS for turbulent wall jet. Recently, Bhattacharjee and Loth [9] simulated laminar and transitional cold wall jets. They have investigated the significance of three different inlet profiles viz. parabolic, uniform and ramp and presented the detailed results of time-averaged wall jet thickness and temperature distribution. They used RANS approach for higher Reynolds number and DNS approach for 3D wall jet.

The stability of 2D free jets was studied experimentally by Sato [10] and Sato and Sakao [11]. Theoretical analysis for axisymmetric free jets was carried out by Batchelor and Gill [12] and Cohen and Wygnanski [13]. Sarma *et al.* [14] have studied 2D incompressible jet development inside a duct in the laminar flow regime for cases with and without entrainment of ambient fluid. While solving for a 3D backward-facing step flow problem, Biswas *et al.* [15] have observed and reported about the evolution of wall jet-like structure in the streamwise and spanwise direction. The self-similarity profile for the streamwise velocity (u) is observed in a plane at a distance of 1.08 away from the sidewall arising due to the sudden expansion near the step. For the spanwise velocity (w), it is at $x = 6$ and 8 which is the culmination of the generation of the w velocity component from the side wall.

Although many studies have been conducted on wall jet, the available literature on theoretical simulation of plane laminar offset jet flows is somewhat limited. The case of an entraining jet located near the jet discharge, which occur in several practical applications, has not been studied. In the present study, a time marching incompressible flow solver has been applied for simulating the flow features of offset jets for a range of aspect ratios and Reynolds number.

2. MATHEMATICAL FORMULATIONS

An incompressible 2D laminar offset jet is considered. For the sake of simplicity, the jet is assumed to be isothermal and having the same density as the ambient fluid. Also, the velocity profile at the jet inlet is taken as parabolic. The governing equations for incompressible laminar flow are solved by stream function-vorticity formulation. The transient nondimensional

governing equations in the conservative form are as follows:

Stream function equation

$$\nabla^2\psi = -\omega \tag{1}$$

Vorticity equation

$$\frac{\partial\omega}{\partial t} + \frac{\partial(u\omega)}{\partial x} + \frac{\partial(v\omega)}{\partial y} = \frac{1}{Re}\nabla^2\omega \tag{2}$$

where ψ-stream function,

$$u = \frac{\partial\psi}{\partial y}, \quad v = -\frac{\partial\psi}{\partial x}, \quad \omega = \frac{\partial v}{\partial x} - \frac{\partial u}{\partial u}$$

The variables are scaled as

$$u = \frac{\bar{u}}{\bar{U}} \quad v = \frac{\bar{v}}{\bar{U}}, \quad x = \frac{\bar{x}}{h}, \quad y = \frac{\bar{y}}{h}, \quad \omega = \frac{\bar{\omega}}{\bar{U}/h}, \quad t = \frac{\bar{t}}{h/\bar{U}}$$

with the over bar indicating a dimensional variable and $\bar{U}, h$ denoting the average jet velocity at nozzle exit and the jet width, respectively.

The boundary conditions needed for the numerical simulation have been prescribed. For an offset jet with entrainment, the following dimensionless conditions have been enforced as shown in Figure 1(b). The inlet slot height is assumed as $h = 0.05\,\text{m}$.

At the jet inlet, along AF (Figure 1(b)),

$$u(y) = 120y - 2400y^2, \quad \omega(y) = 4800y - 120y, \quad \psi(y) = 60y^2 - 800y^3 \tag{3a}$$

Along FE, BA and BC, due to no-slip condition,

$$u = v = 0 \tag{3b}$$

Along ED,

$$\frac{\partial u}{\partial y} = 0 \quad \text{and} \quad \frac{\partial v}{\partial y} = 0 \tag{3c}$$

At downstream boundary, the condition of zero first-derivative has been applied for velocity components. This condition implies that the flow has reached a developed condition. Thus, at (CD),

$$\frac{\partial u}{\partial x} = \frac{\partial v}{\partial x} = 0 \tag{3d}$$

A similar type of boundary conditions has been used by Gu [16] and Al-Sanea [17, 18]. For comparison and validation with available experimental and numerical work, two cases namely, plane wall jet and plane sudden-expansion flow problems have been solved. In the second case, all the walls except the inlet and the outlet are solid. Thus there is no entrainment from the atmosphere and the boundary conditions are no-slip for these surfaces.

3. NUMERICAL PROCEDURE

The unsteady vorticity transport equation (2) in time is solved by alternate direction implicit (ADI) scheme. The central differencing scheme is followed for both the convective as well as the diffusive terms [19]. It consists of two half time-steps.
The first half time-step:

$$\frac{\omega_{i,j}^{n+1/2}-\omega_{i,j}^{n}}{\Delta t/2}+Lx(u\omega)_{i,j}^{n+1/2}+Ly(v\omega)_{i,j}^{n}-\frac{1}{Re}(Lxx(\omega)_{i,j}^{n+1/2}+Lyy(\omega)_{i,j}^{n})=0 \tag{4a}$$

The second half time-step:

$$\frac{\omega_{i,j}^{n+1}-\omega_{i,j}^{n+1/2}}{\Delta t/2}+Lx(u\omega)_{i,j}^{n+1/2}+Ly(v\omega)_{i,j}^{n+1}-\frac{1}{Re}(Lxx(\omega)_{i,j}^{n+1/2}+Lyy(\omega)_{i,j}^{n+1})=0 \tag{4b}$$

where

$$Lx(u\omega)_{i,j}=\frac{(u\omega)_{i+1,j}-(u\omega)_{i-1,j}}{\Delta x_i+\Delta x_{i-1}},\quad Ly(v\omega)_{i,j}=\frac{(v\omega)_{i,j+1}-(v\omega)_{i,j-1}}{\Delta y_j+\Delta y_{j-1}} \tag{5a}$$

$$Lxx(\omega)_{i,j}=\frac{\omega_{i+1,j}-2\omega_{i,j}+\omega_{i-1,j}}{\Delta x_i*\Delta x_{i-1}},\quad Lyy(\omega)_{i,j}=\frac{\omega_{i,j+1}-2\omega_{i,j}+\omega_{i,j-1}}{\Delta y_j*\Delta y_{j-1}} \tag{5b}$$

Equations (4a) and (4b) are rearranged to give the following equations:

$$\begin{aligned}&-(C_x u_{i-1,j}^{n}+S_x)\omega_{i-1,j}^{n+1/2}+(1+2S_x)\omega_{i,j}^{n+1/2}-(-C_x u_{i+1,j}^{n}+S_x)\omega_{i+1,j}^{n+1/2}\\&\quad=(C_y v_{i,j-1}^{n}+S_y)\omega_{i,j-1}^{n}+(1-2S_y)\omega_{i,j}^{n}+(-C_y v_{i,j+1}^{n}+S_y)\omega_{i,j+1}^{n}\end{aligned} \tag{6a}$$

$$\begin{aligned}&-(C_y v_{i-1,j}^{n}+S_y)\omega_{i,j-1}^{n+1}+(1+2S_y)\omega_{i,j}^{n+1}-(-C_y v_{i,j+1}^{n}+S_y)\omega_{i,j+1}^{n+1}\\&\quad=(C_x u_{i-1,j}^{n}+S_x)\omega_{i-1,j}^{n+1/2}+(1-2S_x)\omega_{i,j}^{n+1/2}+(-C_x u_{i+1,j}^{n}+S_x)\omega_{i+1,j}^{n+1/2}\end{aligned} \tag{6b}$$

where

$$C_x=\frac{\Delta t}{2(\Delta x_i+\Delta x_{i-1})},\quad C_y=\frac{\Delta t}{2\left(\Delta y_j+\Delta y_{j-1}\right)},$$

$$S_x=\frac{\Delta t}{Re\Delta x_i*(\Delta x_i+\Delta x_{i-1})},\quad S_y=\frac{\Delta t}{Re\Delta y_j*(\Delta y_j+\Delta y_{j-1})}$$

The discretization of Equation (1) is given by

$$Lxx(\psi) + Lyy(\psi) = -\omega_{i,j} \tag{7}$$

The velocity components are updated by the following equations:

$$u = \frac{\partial \psi}{\partial y} = \frac{\psi_{i,j+1} - \psi_{i,j-1}}{\Delta y_j + \Delta y_{j-1}} \tag{8a}$$

$$v = -\frac{\partial \psi}{\partial x} = \frac{\psi_{i+1,j} - \psi_{i-1,j}}{\Delta x_i + \Delta x_{i-1}} \tag{8b}$$

The velocities (Equations (6a) and (6b)) are calculated at nth time level while advancing to the $(n+1)$th time level. Because of this approximation in the nonlinear terms, the second-order accuracy of the method is somewhat lost. However, something of the second-order accuracy of the linearized system is retained if the velocity field is slowly varying [19].

The discretization is first-order accurate in time and second-order accurate in space $O(\Delta t, \Delta x^2, \Delta y^2)$ and is unconditionally stable. The Poisson Equation (7) is solved explicitly by five point *Gauss–Seidel* methods. *Thom*'s vorticity condition has been used to obtain the wall vorticity as given below.

$$\omega_w = -\frac{2(\psi_{w+1} - \psi_w)}{\Delta n^2} \tag{9}$$

where Δn is the grid space normal to the wall. It has been shown by Napolitano *et al.* [20] and Huang and Wetton [21] that convergence in the boundary vorticity is actually second order for steady problems and for time-dependent problems when $t > 0$. Roache [19] has reported that for a Blausius boundary-layer profile, numerical test verify that this first-order form is more accurate than the second-order form.

At the bottom wall and the left-side wall, constant streamlines are assumed based on inlet flow. At the outlet in the downstream direction, streamwise gradients are assumed to be zero. At the entrainment boundary, normal velocity gradient is zero [22].

The detailed boundary conditions are
along FE (Figure 1(b)),

$$\omega(y) = \frac{2(\psi_w - \psi_{w+1})}{\Delta x_1 * \Delta x_1}, \quad \psi = 0.05 \tag{10a}$$

along BA,

$$\omega(y) = \frac{2(0 - \psi_{w+1})}{\Delta x_1 * \Delta x_1}, \quad \psi = 0 \tag{10b}$$

along BC,

$$\omega(x) = \frac{2(0 - \psi_{w+1})}{\Delta y_1 * \Delta y_1}, \quad \psi = 0 \tag{10c}$$

along ED,

$$\frac{\partial^2 \psi}{\partial x \partial y} = 0 \tag{10d}$$

$$\psi_{i,j} = \psi_{i-1,j} + \psi_{i,j-1} - \psi_{i-1,j-1} \tag{10e}$$

$$u_{i,j} = u_{i,j-1} \tag{10f}$$

$$v_{i,j} = v_{i,j-1} \tag{10g}$$

$$\omega_{i,j} = \frac{v_{i+1,j} - v_{i-1,j}}{\Delta x_i + \Delta x_{i-1}} \tag{10h}$$

Along CD,

$$\psi_{i,j} = 2\psi_{i-1,j} - \psi_{i-2,j} \tag{10i}$$

$$\omega_{i,j} = \omega_{i-1,j} \tag{10j}$$

$$u_{i,j} = u_{i-1,j} \tag{10k}$$

$$v_{i,j} = v_{i-1,j} \tag{10l}$$

Equation (10d) is also followed by Rao *et al.* [23] for entrainment boundary.

Solution approaches steady-state asymptotically while the time reaches infinity. The computational domain considered here is clustered cartesian grids. For unit length, the grid space at ith node is [24],

$$x_i = \left(\frac{i}{i_{\max}} - \frac{\kappa}{\upsilon} \sin\left(\frac{i\upsilon}{i_{\max}} \right) \right) \tag{11}$$

where υ is the angle and κ is the clustering parameter. $\upsilon = 2\pi$ stretches both end of the domain whereas $\upsilon = \pi$ clusters more grid points near one end of the domain. κ varies between 0 and 1. When it approaches 1, more points fall near the end.

For $Re = 200$, a time step of 0.0001 is used. The results obtained for lower Re steady-state solution have been used as initial guess value for high Re flow for stream function and vorticity. Thus a higher time step of 0.001 is used for $Re > 200$. This is based on the procedure given by Comini *et al.* [25]. It has been observed that for coarse grids, larger time step can be used whereas for fine grids, the solution diverges with large time step. While selecting κ, time step also needs to be considered. The maximum vorticity error behaviour is complicated as explained by Roache [19]. While marching in time for the solution, it has been observed that the maximum vorticity error gradually decreases. It then increases drastically and finally decreases asymptotically leading to steady-state solution. The convergence criteria to be set in such a way that it should not terminate at false stage. At steady state, the error

reaches the asymptotic behaviour. Here it is set as sum of vorticity error reduced to either the convergence criteria ε or large total time.

$$\sum_{i,j=1}^{i_{\max},j_{\max}} (\omega_{i,j}^{t+\Delta t} - \omega_{i,j}^{t}) < \varepsilon \tag{12}$$

4. VALIDATION OF THE CODE

To validate the developed code, the 2D lid-driven square-cavity flow problem [26] and the backward-facing flow problem [27, 28] have been solved. Excellent agreement has been obtained with the benchmark solutions reported in the above references. The laminar plane wall jet problem (Figure 2) then has been solved and the computed velocity profiles are compared with the similarity solutions of Reference [2] and the experimental results of Reference [7] in a similar way as represented by Seidel [8] (Figure 3).

For sudden expansion flow investigation, the computational domain reported by Durst *et al.* [29] is considered. The domain chosen is $50H$ in length and expansion ratio is 2. The schematic diagram of the problem is shown in Figure 4(a). Grids have been clustered similar to that of Reference [30]. At inlet, parabolic velocity profile is assumed and no-slip conditions are assumed along the solid walls. At exit, streamwise gradients are assumed as zero for the vorticity and u velocity component [19]. For different Re, the u velocity component at various downstream locations is compared with experimental and numerical prediction of Reference [29]. For $Re = 70$, the flow is symmetric. Flow separates at the corner of the inlet and reattaches at the top and bottom of the solid wall (Figure 4(b)). Results are having

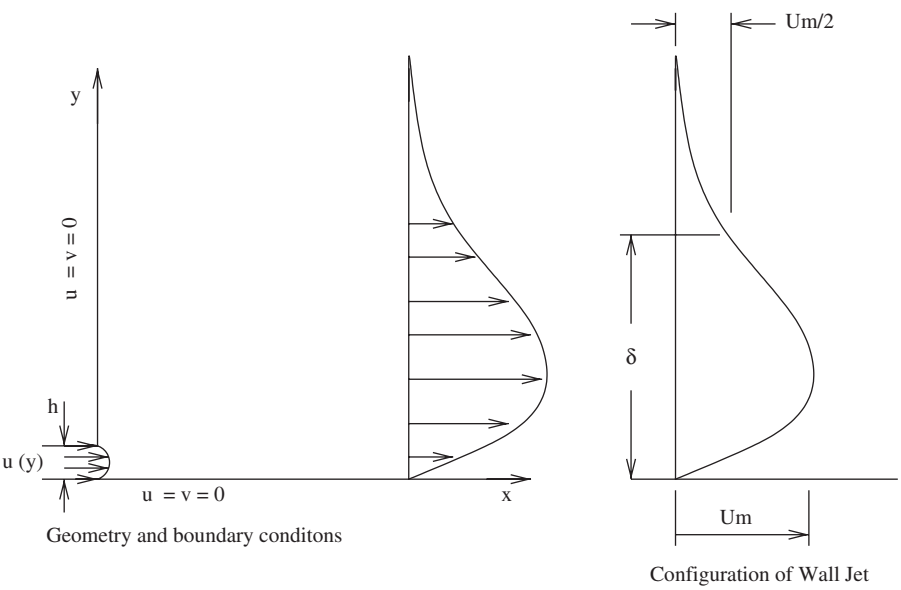

Figure 2. Schematic diagram and boundary conditions of a wall jet problem.

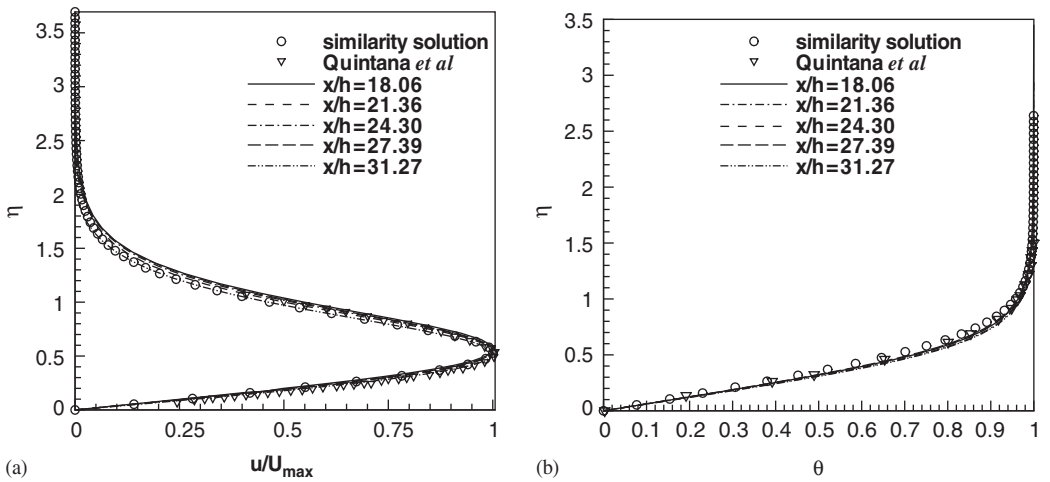

Figure 3. Laminar wall jet results. $Re = 500$, $Pr = 1.4$: (a) u-velocity; and (b) temperature.

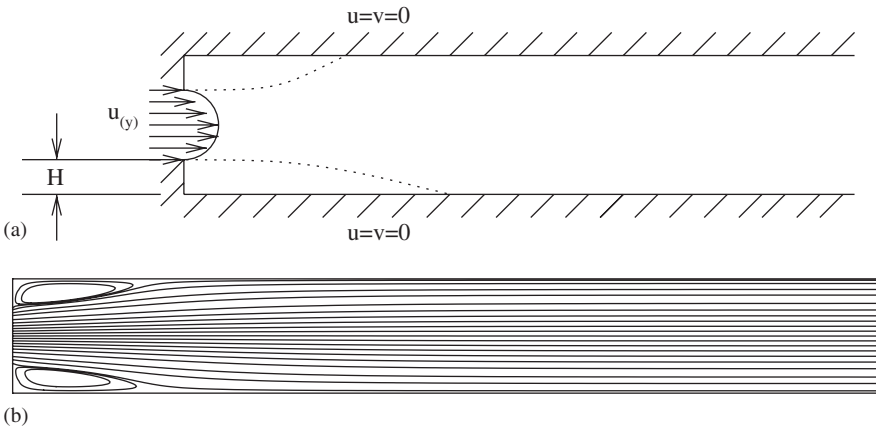

Figure 4. Plane sudden-expansion flow problem: a part of the domain [29]: (a) schematic diagram and boundary conditions; and (b) stream line contour $Re = 70$.

good agreement at locations $x/H = 3.6$ and $x/H = 14$, whereas at $x/H = 5$ along the symmetry line there are some deviations (Figure 5). For $Re = 610$, the comparisons of the axial velocity profiles are shown in Figure 6. The present numerical predictions are close to their predicted values at downstream locations ($x/H = 14$, $x/H = 29$) and ($x/H = 44$). The present computations captures the formation of second recirculation at top wall for this Re, which is consistent with References [29, 30].

Sarma *et al.* [14] validated their result for a critical $Re = 190$ with a critical $Re = 187$ of Reference [31]. Here no such attempt has been made to compare the results with an adjustment

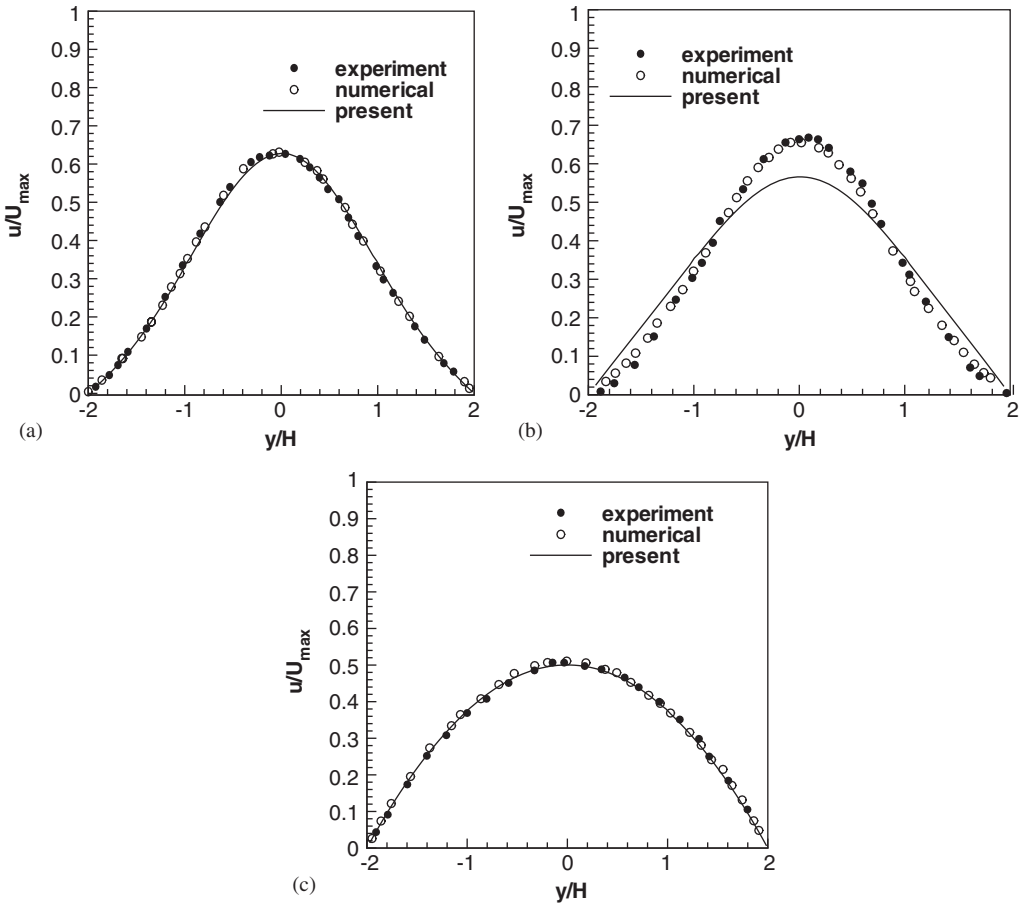

Figure 5. Comparison of normalized u velocity profiles for $Re = 70$ [29]: (a) $x/H = 3.6$; (b) $x/H = 5$; and (c) $x/H = 14$.

of Re. The deviations in the results of the present study and those of the earlier investigations may be attributed to the differences in the numerical scheme and the round off/discretization errors [14].

5. GRID-INDEPENDENT STUDY

The domain has been chosen as $30 \times h$ in streamwise direction and $20 \times h$ in normal direction. Systematic grid refinement study is carried out with $39 \times 31, 51 \times 41, 61 \times 61, 71 \times 61, 81 \times 81$ and 101×101 (Figure 7). Grid refinement level 5 is used for the entire computations. The grids are clustered in streamwise direction whereas in normal direction up to $3 \times h$ height, grids are arranged uniformly and above this region, they are clustered. Typical grids are shown in Figure 8.

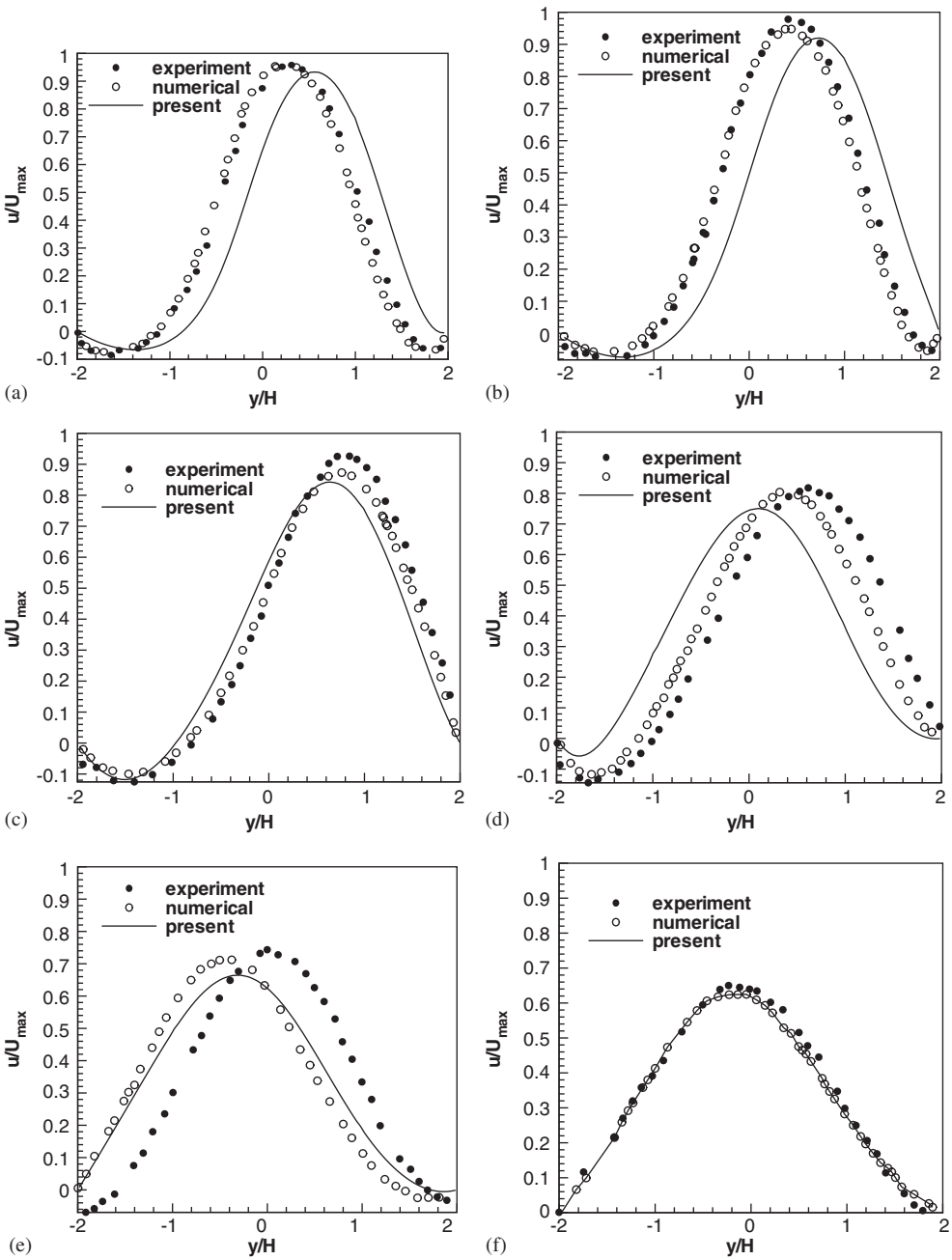

Figure 6. Comparison of normalized u velocity profiles for $Re = 610$ [29]: (a) $x/H = 3.6$; (b) $x/H = 5$; (c) $x/H = 14$; (d) $x/H = 20$; (e) $x/H = 29$; and (f) $x/H = 44$.

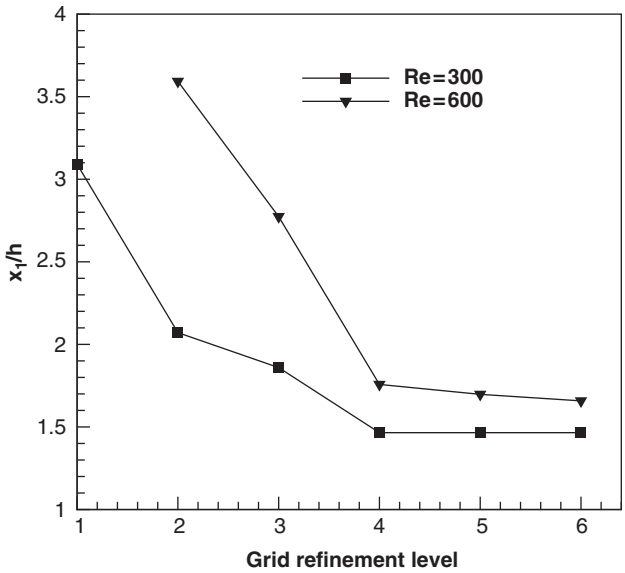

Figure 7. Grid independence study, OR = 1.0.

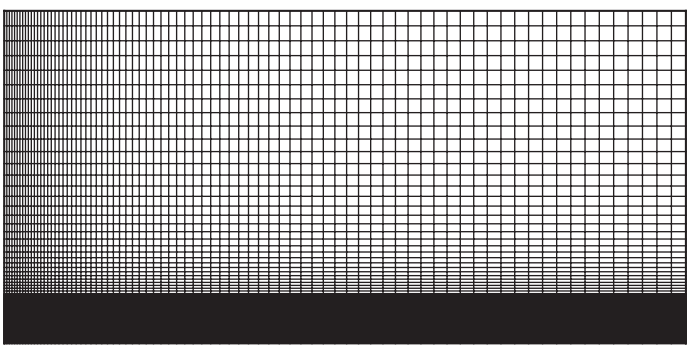

Figure 8. Typical grids used for an offset jet OR = 1.0.

6. RESULTS AND DISCUSSION

Flow separates at the corner and reattaches at the bottom of the wall due to Coanda effect. This length is called the reattachment length (x_1, Figure 1(a)). The entire region can be divided into three sub-regions as recirculation region, impingement region and wall jet region. To understand the flow physics, two parameters considered here are *Re* and offset ratio (OR). Offset ratio is defined as the ratio of step height (H) to inlet slot height (h). Results are presented here for three OR viz. OR = 0.5, 1.0, 1.5 and *Re* is varied from 200 to 600 in steps

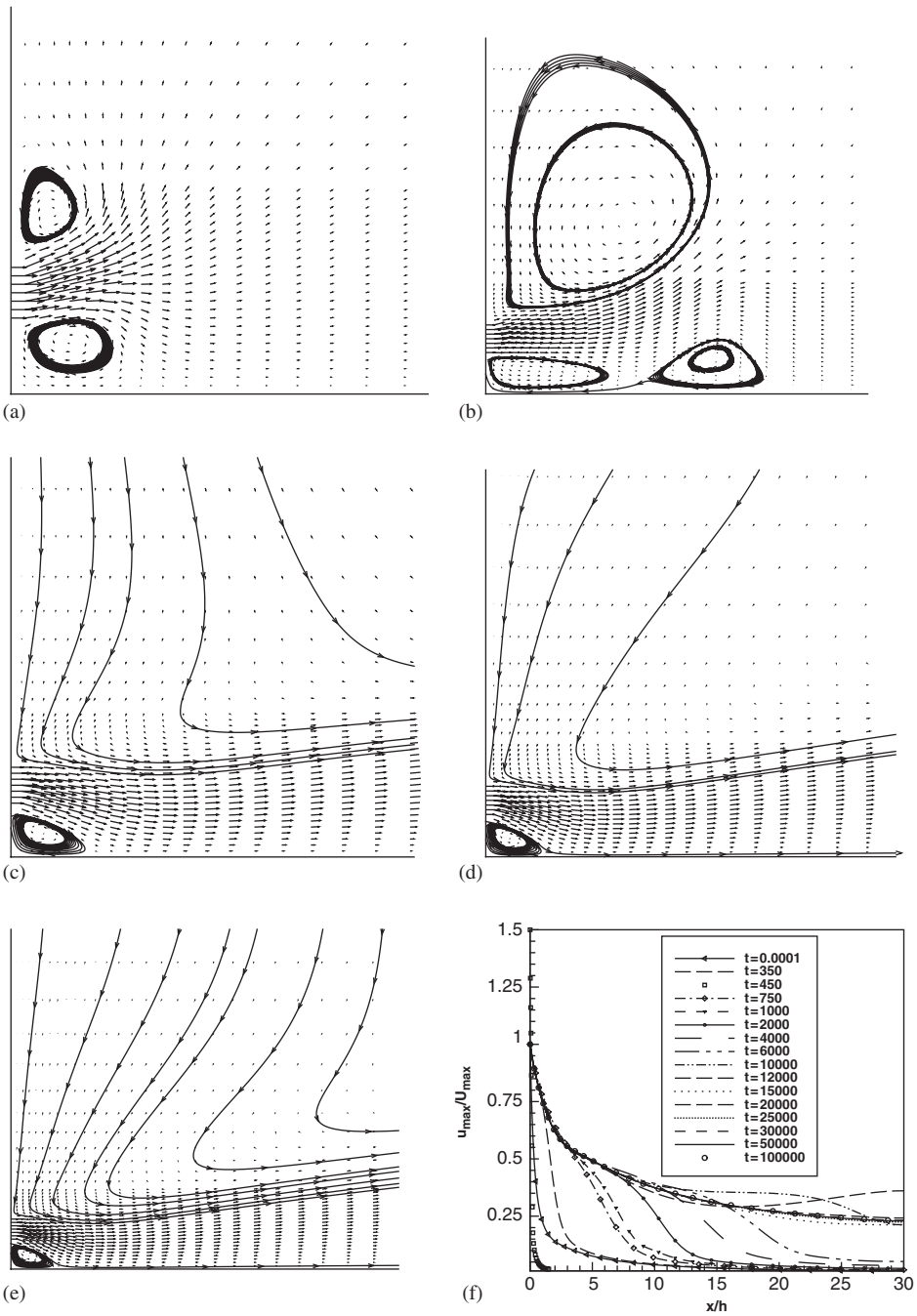

Figure 9. Velocity vector and stream trace plot: (a) $t = 350$; (b) $t = 750$; (c) $t = 10\,000$; (d) $t = 20\,000$; (e) $t = 3 \times 10^4$; and (f) transient results of local u_{max} distribution, $Re = 600$; OR = 1.0.

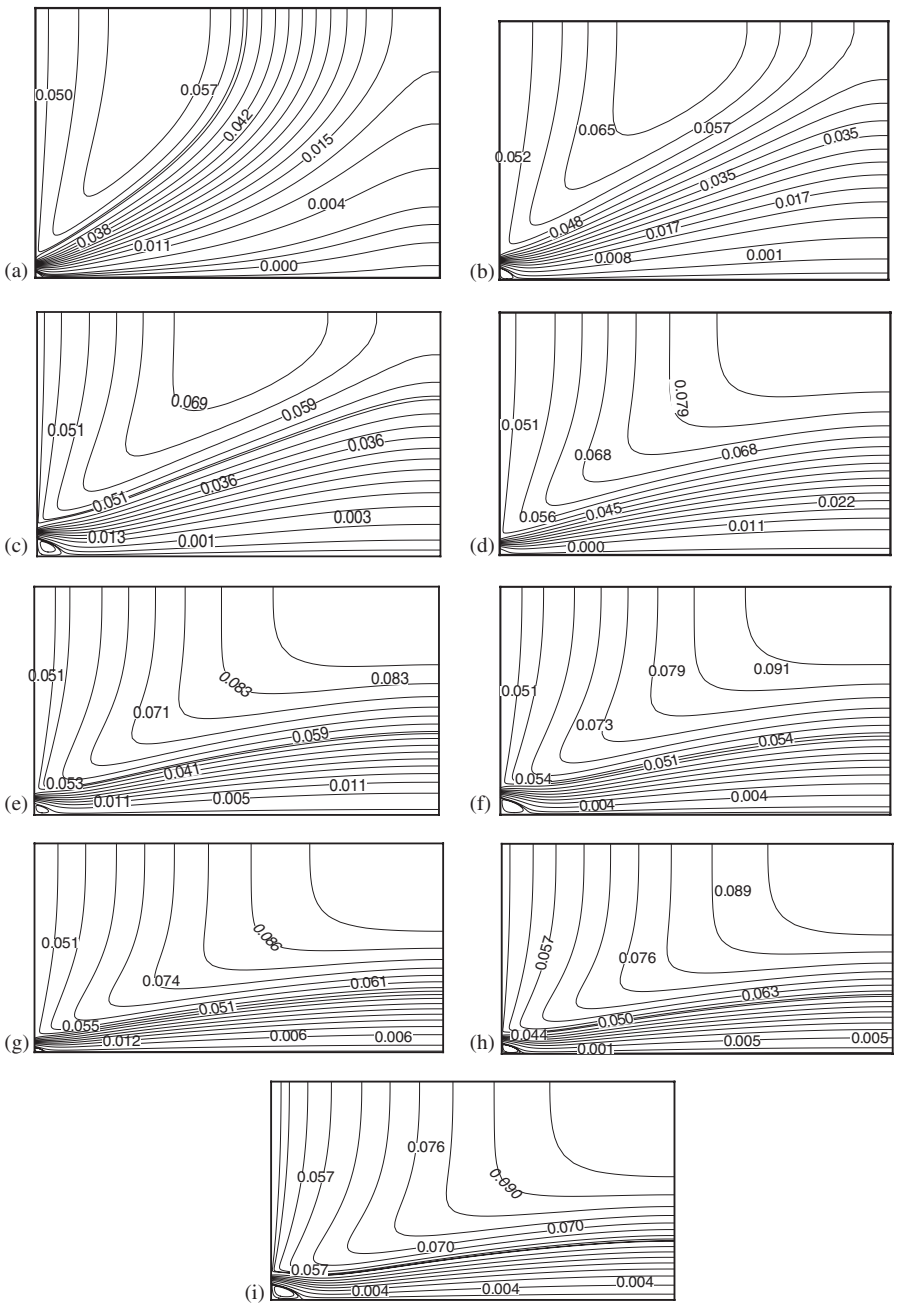

Figure 10. Effect of offset ratio and Re on the streamline pattern: (a) $Re = 200$, OR $= 0.5$; (b) $Re = 200$, OR $= 1.0$; (c) $Re = 200$, OR $= 1.5$; (d) $Re = 300$, OR $= 0.5$; (e) $Re = 300$, OR $= 1.0$; (f) $Re = 300$, OR $= 1.5$; (g) $Re = 400$, OR $= 0.5$; (h) $Re = 400$, OR $= 1.0$; and (i) $Re = 400$, OR $= 1.5$.

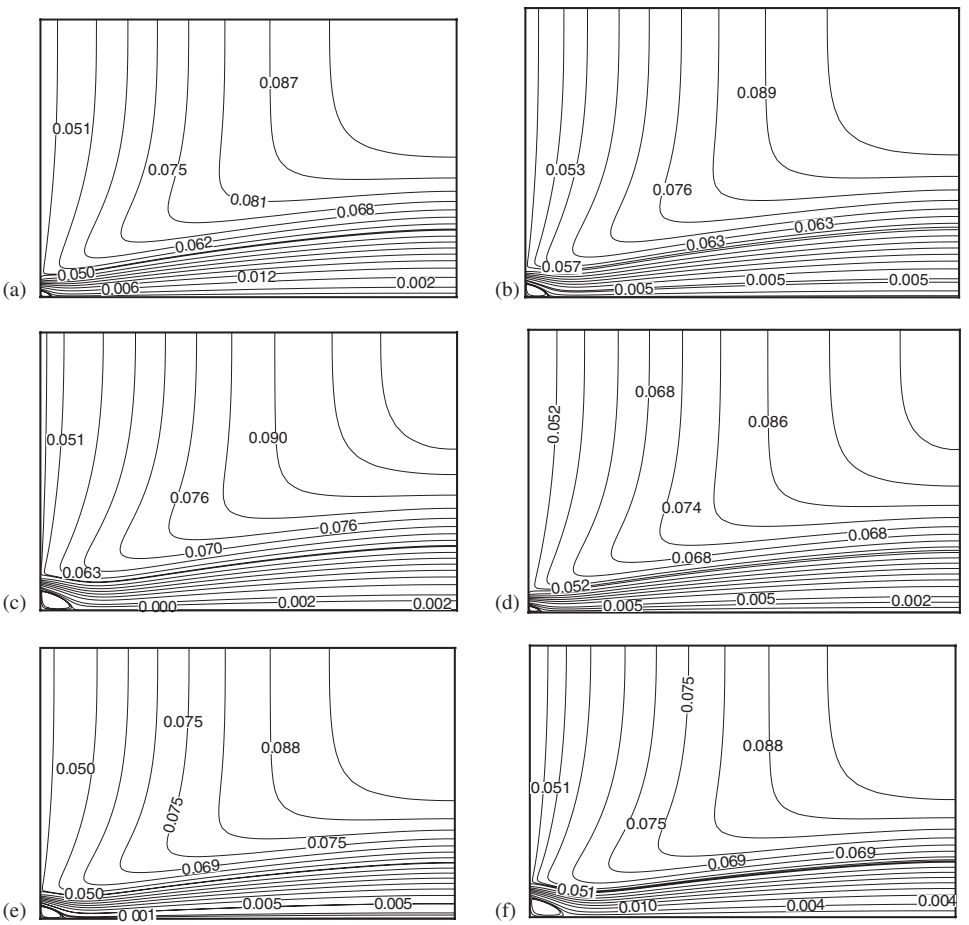

Figure 11. Effect of offset ratio and Re on the streamline pattern: (a) $Re = 500$, OR $= 0.5$; (b) $Re = 500$, OR $= 1.0$; (c) $Re = 500$, OR $= 1.5$; (d) $Re = 600$, OR $= 0.5$; (e) $Re = 600$, OR $= 1.0$; and (f) $Re = 600$, OR $= 1.5$.

of 50. Since the clustered grids are used for the computations, Tecplot 9.0 [32] is used for extracting the values for any particular location.

In the problem of a nonbuoyant offset jet, a slot jet is discharged parallel to a solid wall. After leaving the nozzle, the jet curves towards the boundary and attaches to it, enclosing an eddying region of separated flows as shown in Figure 1(a). This phenomenon is caused by the reduction of pressure on the inner side of the jet due to entrainment of fluid by the jet. Flow fields, velocity profiles, jet trajectories and attachment length (cavity length) are investigated through detailed velocity measurements. Presented in Figure 9 are numerically simulated velocity vectors representing the flow fields of an offset jet at various time levels for an offset ratio of 1.0 and Reynolds number 600. It can be seen that the initial action of

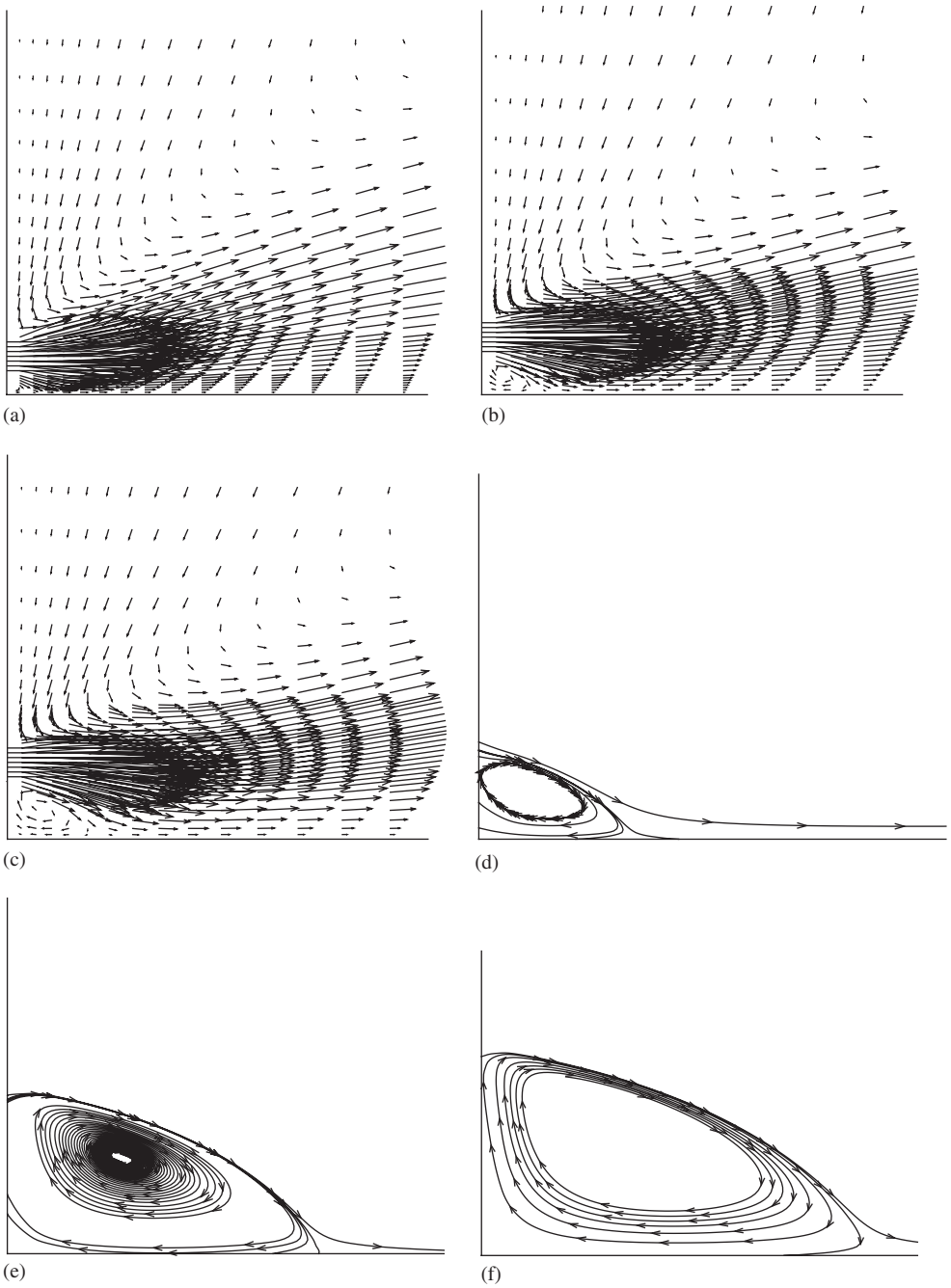

Figure 12. (a–c) Velocity vector and (d–f) the recirculation eddy, $Re = 300$: (a) OR = 0.5; (b) OR = 1.0; (c) OR = 1.5; (d) OR = 0.5; (e) OR = 1.0; and (f) OR = 1.5.

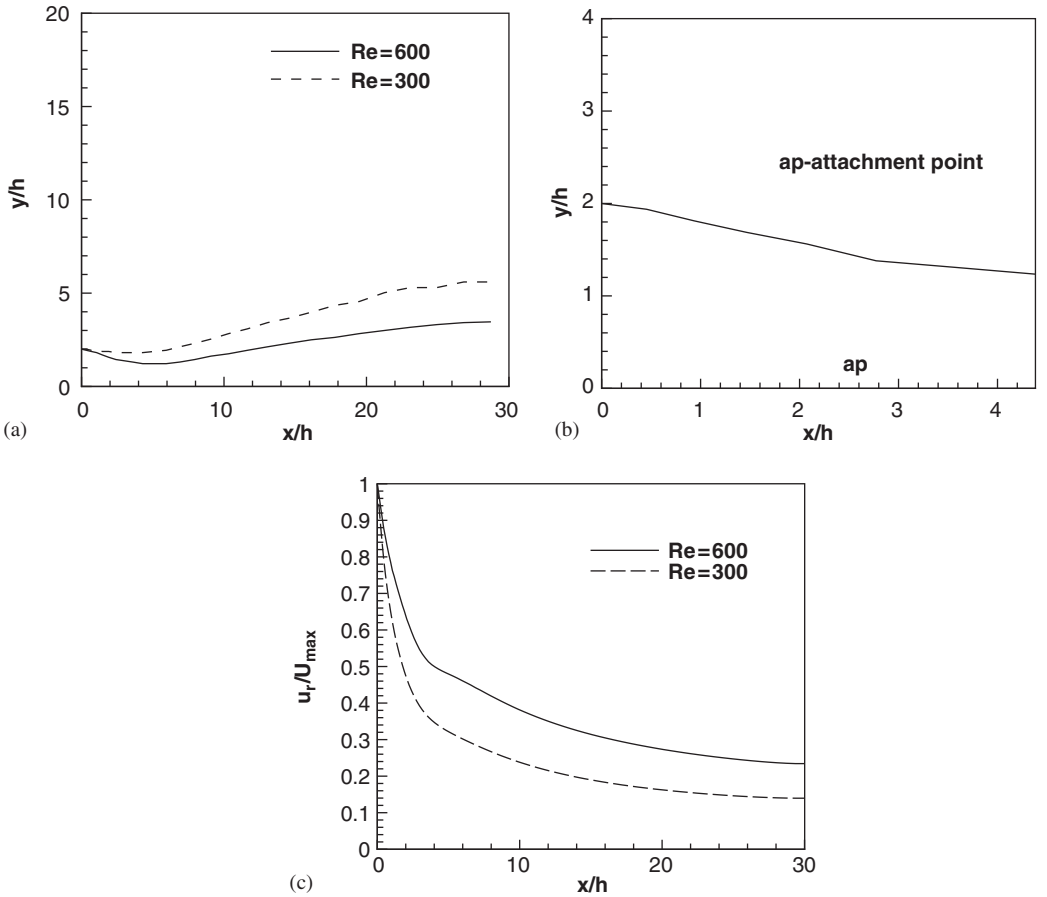

Figure 13. Centreline velocity: OR = 1.5: (a) u_{max} location; (b) u_{max} trajectory: $Re = 600$; and (c) centreline velocity.

the offset jet that enters the stationary ambient fluid is similar to that of a free jet, entraining fluid from the ambient and forming pair of vortices on two sides of the jet at $t = 350$ (Figure 9(a)). A recirculation contained by the lower portion of the jet, the bottom, and the vertical wall is established by the entraining effect of the jet. Evidence of a secondary recirculation in the lower region at this stage is also shown in Figure 9(b) at a time $t = 750$. The jet is deflected towards the bottom boundary to which the jet is closer due to the Coanda effect at a larger time ($t = 10\,000$, Figure 9(c) and at $t = 20\,000$, Figure 9(d)). The flow (attachment and recirculation) achieves its steady state at $t = 30\,000$. The secondary recirculation near the bottom boundary is pushed downstream and disappears after the flow becomes stable (Figure 9(e)).

During the process of flow establishment, the entrainment of ambient fluid is reduced along the inner edge due to a finite volume of fluid and enhanced along the outer edge of the jet,

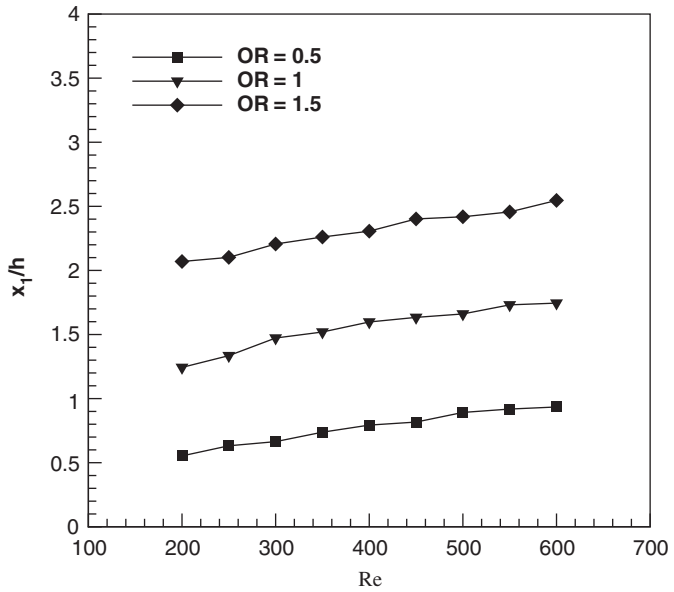

Figure 14. Comparison of reattachment length with *Re* and OR.

eventually causing attachment of the jet to the boundary. The surrounding fluid above the jet being entrained into the jet is replenished by ambient fluid in the farther field. A recirculation contained by the upper part of the jet, the top boundary, and the vertical wall is formed as shown in Figure 9(a). This upper vortex, which is initially ($t = 350$) above the jet and symmetric to the lower one about the jet centreline, moves downstream and stretches in the horizontal direction during the flow attachment and stabilization. A back flow is expected to occur at the upper portion of the out flow boundary to complete the large upper recirculation. Transient results of normalized $u_{\max}$ are shown in Figure 9(f). It is noticed that the solution reaches steady state condition gradually. However, there are few oscillations at $t = 10\,000$ and 20 000. Further investigation in time show that the solution becomes time independent at $t = 30\,000$. It is ensured by computing up to large total time of $t = 10^5$.

Figures 10 and 11 illustrate the streamline plots for various *Re* and OR. It is observed that while *Re* increases the size of recirculation eddy increases. Also it is noticed that similar effect is obtained when OR is increased. At exit, the streamlines become parallel and thus our assumption for fully developed flow is satisfied. It is of interest to note that the streamline pattern for $Re = 200$, $\mathrm{OR} = 0.5$ Figure 10(a) is different from others. The main flow is unable to overcome the friction and thus is spreading in the normal direction. Similar observations have been made by Chiriac and Ortega [33] for low *Re* case in a confined slot jet impingement flow. Near the bottom wall, streamlines are less denser in order to satisfy the no-slip conditions along the walls. However, the streamlines are denser throughout the impingement region. A part of the entrainment streamlines are passed towards the jet ejecting location and it shears with outer layer of the main flow. A close view of the recirculation eddies for $Re = 300$ and $\mathrm{OR} = 0.5, 1.0$ and 1.5 are shown with velocity vector plot in Figure 12. The location of $u_{\max}$

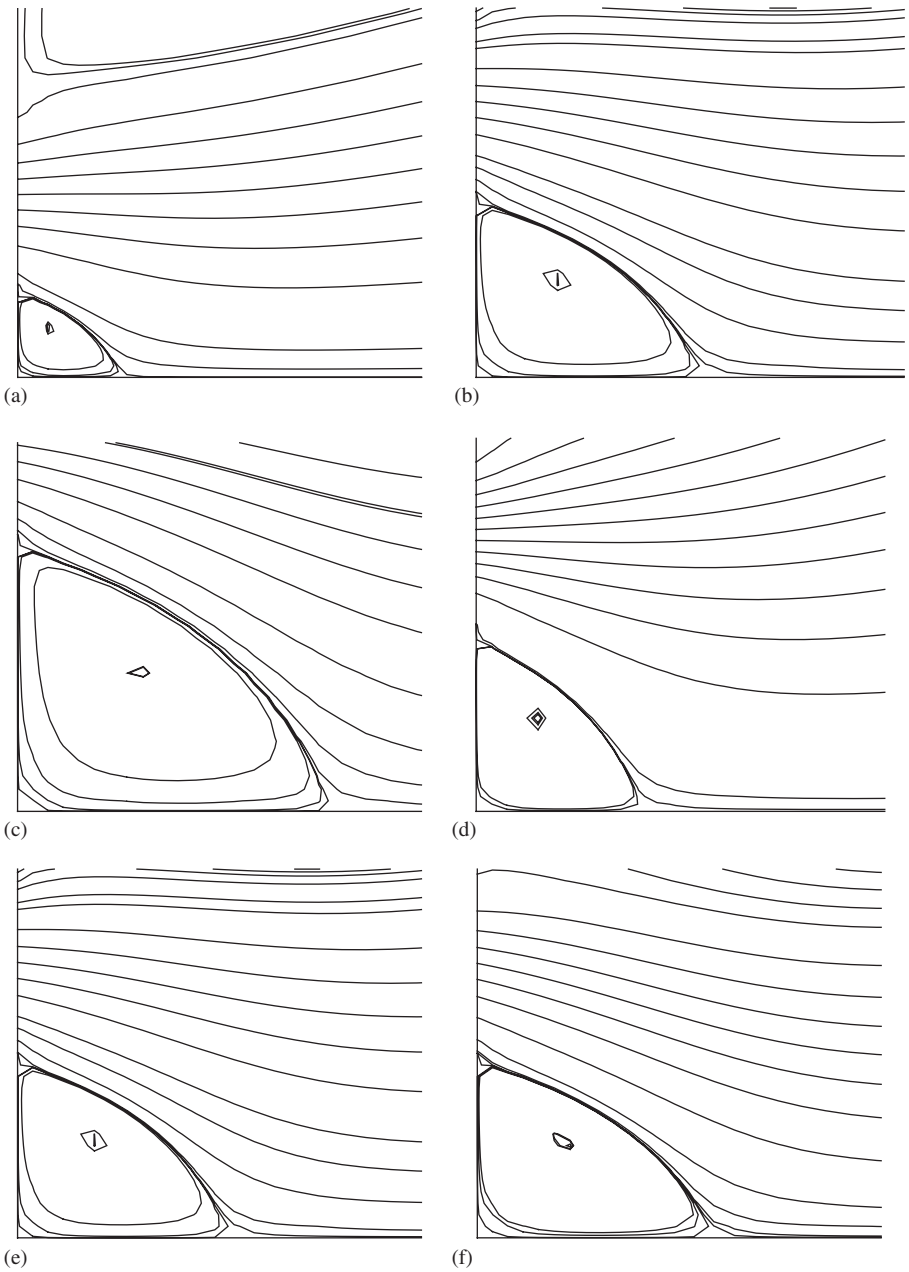

Figure 15. Recirculation eddy structure for various Re and OR: (a) $Re = 400$; OR $= 0.5$; (b) $Re = 400$, OR $= 1.0$; (c) $Re = 400$, OR $= 1.5$; (d) $Re = 200$, OR $= 1.0$; (e) $Re = 400$, OR $= 1.0$; and (f) $Re = 600$, OR $= 1.0$.

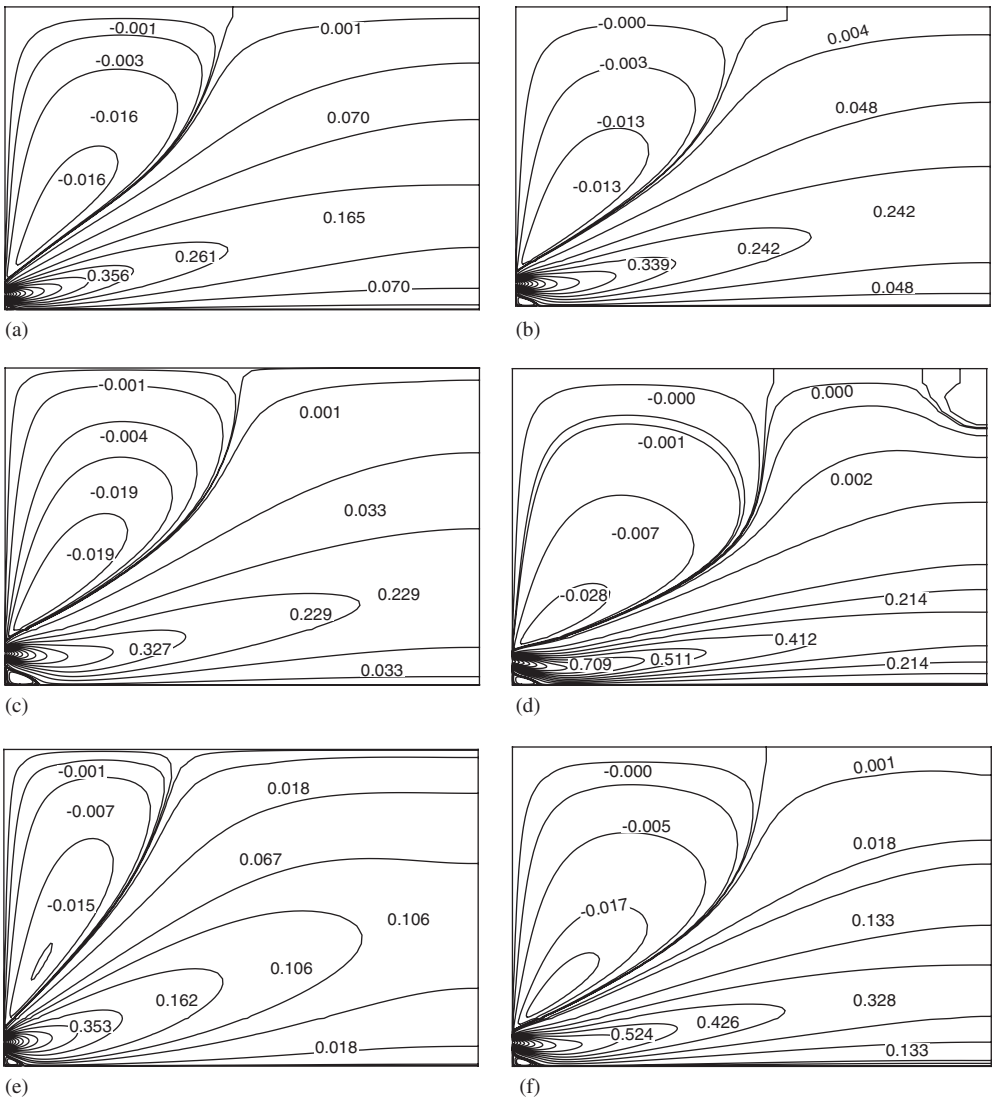

Figure 16. Effect of OR and Re on entrainment. u-velocity contour plot: (a) OR $= 0.5$, $Re = 300$; (b) OR $= 1.0$, $Re = 300$; (c) OR $= 1.5$, $Re = 300$; (d) $Re = 200$, OR $= 1.0$; (e) $Re = 400$, OR $= 1.0$; and (f) $Re = 600$, OR $= 1.0$.

for the entire length of the domain is shown in Figure 13(a). The y/h location is gradually falling down towards the bottom wall and after reattachment point it increases in rest of the domain length. This is attributed due to the jet deflection up to the reattachment point because of the Coanda effect. After that, it spreads in the downstream direction like a wall jet. The jet trajectory is defined as the position of locus of maximum centreline velocity as given by

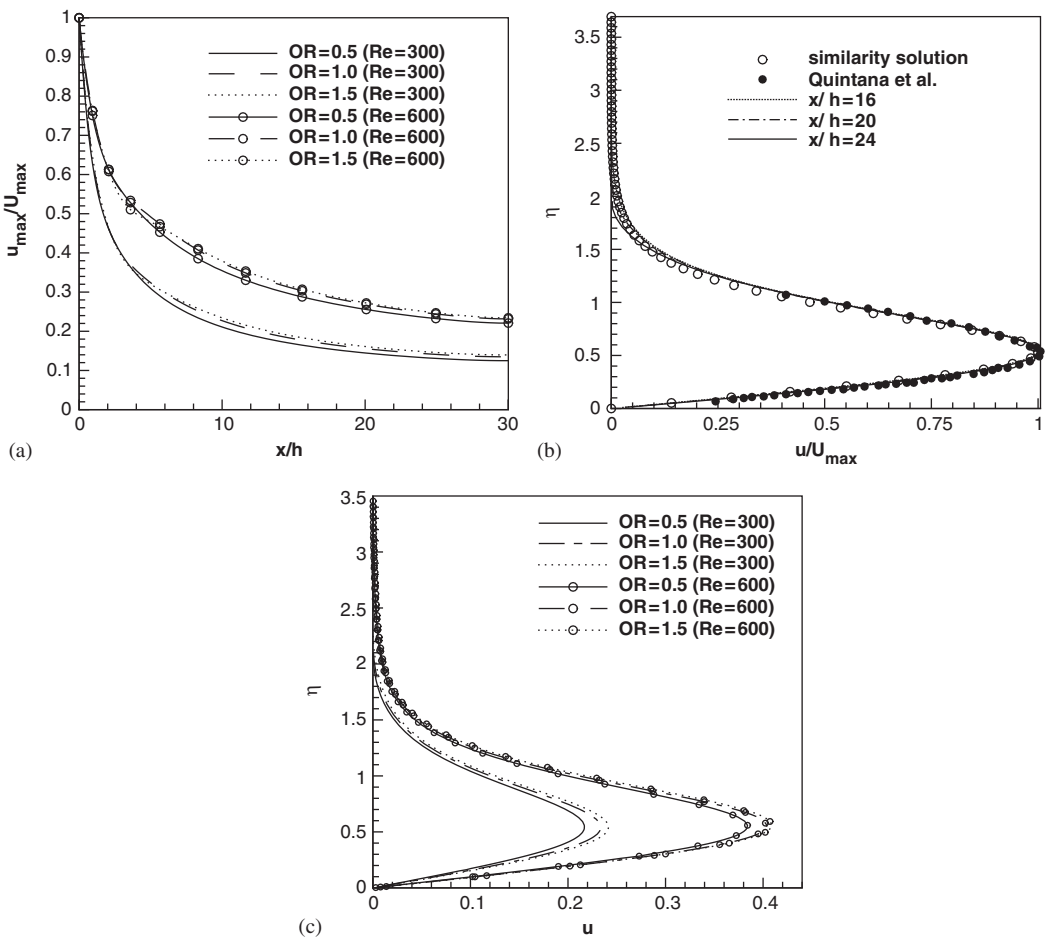

Figure 17. Local u velocity comparison: (a) local u maximum velocity decay; (b) comparison of u-velocity profile ($Re = 300$, OR $= 1$); and (c) u-velocity at wall jet region ($x/h = 20$).

Gu [16] and shown in Figure 13(b). Variation of the jet centreline velocity with distance is shown in Figure 13(c). The jet centreline velocity decreases gradually in downstream direction. However, at high Re ($= 600$), a small kink is present after the reattachment point. It is attributed to the decrease in pressure after the reattachment of the jet.

The dependency of x_1/h with Re and OR is shown in Figure 14. The reattachment length has an increasing trend with Re with a falling rate of increase within the range of Re considered. It is noticed that the centre of the eddy moves away from the solid walls with Re and OR. However, it is observed that the x direction variation is higher if Re increases while y direction variation is higher if OR increases (Figure 15).

Entrainment occurs when a jet ejects into quiescent medium. Low pressure is created above and below, near the mouth of the jet ejection. The ambient fluid flows towards it and

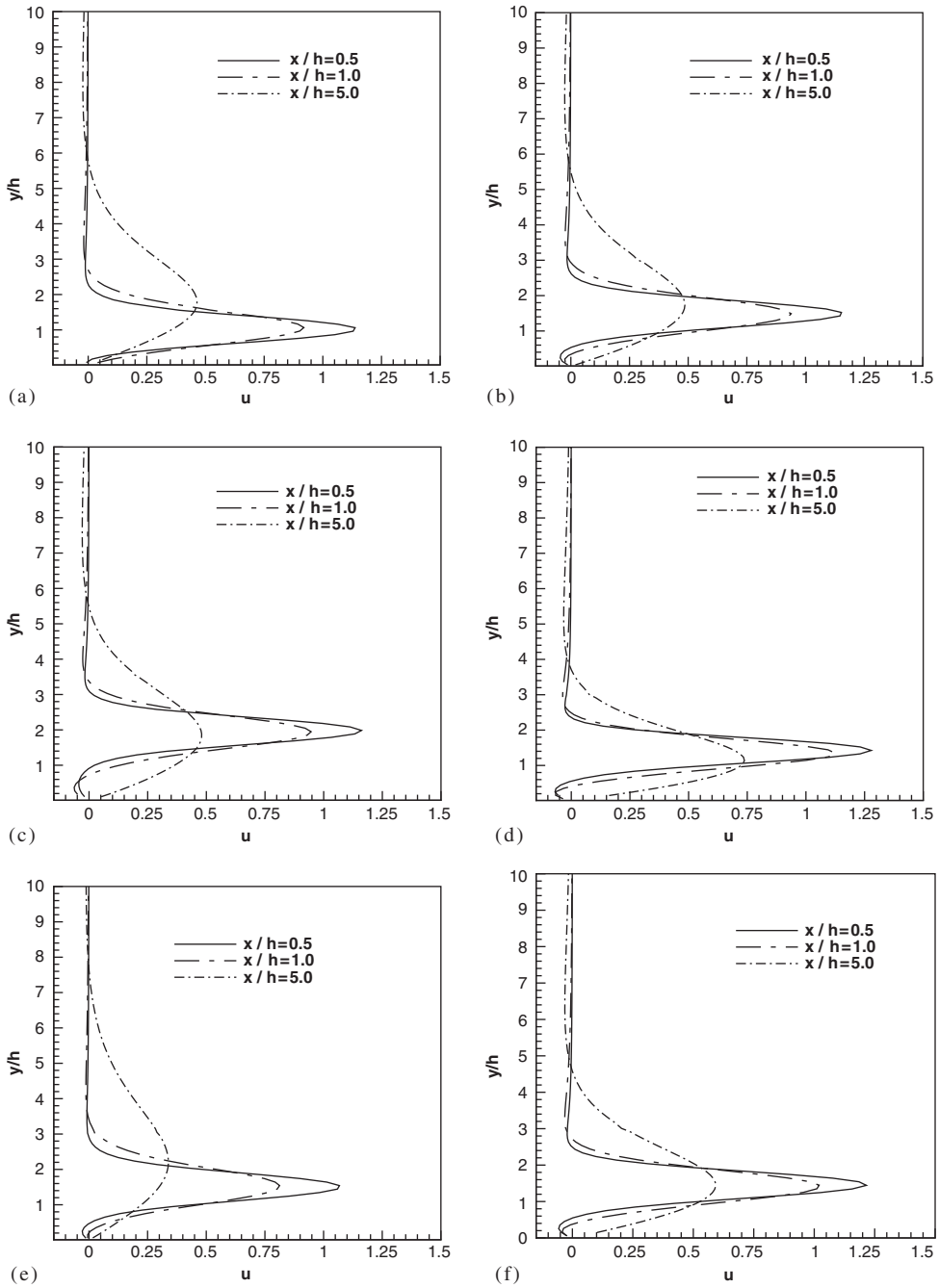

Figure 18. u-velocity component for various Re and OR: (a) $Re = 300, \mathrm{OR} = 0.5$; (b) $Re = 300$, OR $= 1.0$; (c) $Re = 300$, OR $= 1.5$; (d) $Re = 200$, OR $= 1.0$; (e) $Re = 400$, OR $= 1.0$; and (f) $Re = 600, \mathrm{OR} = 1.0$.

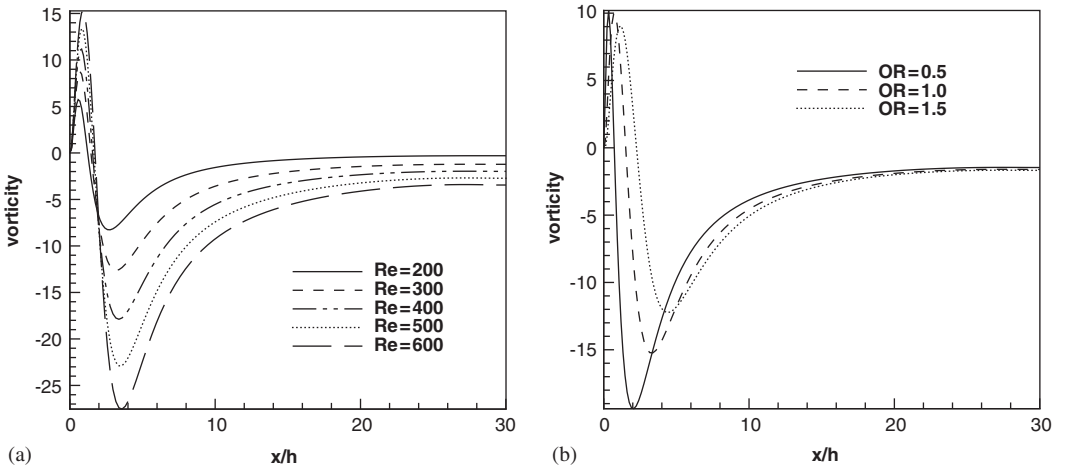

Figure 19. Vorticity distribution along the bottom wall: (a) OR = 1.0; and (b) $Re = 350$.

shear with the main flow. These phenomena are well captured in the present computations (Figure 16). The negative u velocity contours show the ambient fluid flow towards low pressure zone created by the ejection of the jet. It is noticed that this flow rate is increased when OR is increased, and it increases markedly with Re. The agreement of the numerical solution with wall jet similarity solution is expected where the u velocity turns positive everywhere in the normal direction. The region from reattachment point to this length is called impingement region. After impingement, the pressure of the main flow starts to decrease in this region. The decay of normalized local $u_{\max}$ is shown in Figure 17(a). The decay of $u_{\max}/U_{\max}$ is linear and independent of OR in the recirculation region. However, it is higher for low Re. This is mainly due to the sudden expansion and interaction of the jet with ambient entrainment fluid. Further downstream the decay follows common behaviour for various OR and Re. It is noticed that at higher OR, decay becomes independent of OR but a function of Re.

The computed u velocity profile at different downstream locations is compared with the similarity solution and experimental results of Reference [7] for laminar wall jet. It shows very good agreement with them (Figure 17(b)). It satisfies the momentum flux, Glauert constant for laminar wall jet [2]. Local u velocity is compared for different Re and OR at $x/h = 20$ (Figure 17(c)). When OR increases for a particular Re, an increase in local $u_{\max}$ is attributed due to large reattachment length which reduces the decay of u-velocity. However, the difference is reduced at higher OR. It is observed that the jet spreads more in the normal direction for low Re than at high Re. Spreading of jet is demonstrated near the impingement region by u velocity profile (Figure 18). $u_{\max}$ is not much affected by OR in this particular region (Figure 18(a)–(c)). At low Re, jet spreads more at particular location, for example $x/h = 5$ which is evident from Figure 18(d)–(f). This is due to the relatively less amount of momentum being carried by a lower Re case. An increase in $u_{\max}$ is obvious when Re increases.

The bottom wall vorticity distributions for different Re with OR = 1.0 are shown in (Figure 19(a)). Near the impingement region the vorticity variations are large while in

downstream direction it becomes independent of x. It is noticed that while Re increases the normal u velocity gradient is increased, which influences the vorticity in the negative direction. Also the wall vorticity is higher (in negative side) because the velocity gradient near the wall is higher. Figure 19(b) shows the wall vorticity distribution for various OR and $Re = 350$. Also it is noticed that the OR affects the vorticity up to the impingement region and further downstream, vorticity becomes independent of OR. This implies that the adjustment of the nonuniformity created by offset is complete near the outlet.

7. CONCLUSIONS

Two-dimensional incompressible nonbuoyant offset jet is solved by stream function and vorticity formulation considering the problem as asymptotic solution to the transient equation. The flow characteristics like strength of recirculation eddy, impingement length, decay of local velocity and wall jet region are studied in details by varying Re and offset jet ratio. The transient results show the nature of vortex generation, its movement with respect to time, disappearance of the outside vortex and attainment of the final steady-state distribution. The location of $u_{\max}$ is presented. The entrainment is increased for high Re and it is less affected with change in OR. The reattachment length has an increasing trend with Re with a falling rate of increase within the range of Re considered. The centre of recirculation shifts significantly in the downstream direction with increase in Re. However, it moves in the normal direction if OR is increased. The decay rate of u is not much affected by OR near the impingement region. However, at high OR, solution becomes independent of OR. Far downstream direction, flow behaves like a wall jet flow. The similarity u velocity profiles are having excellent agreement with experimental and numerical predictions. A shift in normal direction is observed in $u_{\max}$ while OR increases. The boundary layer thickness is smaller while Re increases. The bottom wall vorticity is considerably affected near the impingement region. In far downstream it becomes independent of a particular Re. The absolute vorticity value increases with an increase in Re.

NOMENCLATURE

h	inlet slot height, m
i	x-direction grid point
j	y-direction grid point
n	normal direction
Re	Reynolds number for the fluid
$\bar{t}$	dimensional time, s
t	nondimensional time
$\bar{U}$	inlet mean velocity, m/s
u_r	dimensionless resultant velocity
$\bar{u}, \bar{v}$	dimensional velocity components along $(\bar{x}, \bar{y})$ axes, m/s
u, v	dimensionless velocity components along (x, y) axes

$\bar{x}, \bar{y}$ dimensional Cartesian co-ordinates along and normal to the plate, m
x, y dimensionless Cartesian co-ordinates along and normal to the plate

Greek letters

δ wall jet boundary layer thickness
ε convergence criterion
η similarity variable
κ clustering parameter
υ dimensionless stream function
ω dimensionless vorticity

Subscripts

max maximum
w wall

ACKNOWLEDGEMENTS

The helpful comments of the reviewers are sincerely acknowledged by the authors.

REFERENCES

1. Tritton DJ. *Physical Fluid Dynamics*. Von Nostrand Reinhold: New York, U.K., 1977; 284–286.
2. Glauert MB. The wall jet. *Journal of Fluid Mechanics* 1956; **1**(1):1–10.
3. Schlichting H, Gersten K. *Boundary Layer Theory* (8th revised edn). Springer: Berlin, 2000; 215–218.
4. Chandrasekhara Swamy NV, Bandyopadhyay P. Mean and turbulent characteristics of three-dimensional wall jets. *Journal of Fluid Mechanics* 1975; **1**(3):541–562.
5. Cohen J, Amitay M, Bayly BJ. Laminar-turbulent transition of wall-jet flows subjected to blowing and suction. *Physics of Fluids A* 1992; **4**(2):283–289.
6. Amitay M, Cohen J. Instability of a two-dimensional plane wall jet subjected to blowing or suction. *Journal of Fluid Mechanics* 1997; **344**:67–94.
7. Quintana DL, Amitay M, Ortega A, Wygnanski IJ. Heat transfer in the forced laminar wall jet. *Journal of Heat Transfer* 1997; **119**:451–459.
8. Seidel J. Numerical investigations of forced laminar and turbulent wall jets over a heated surface. *Ph.D. Thesis*, Faculty of the Department of Aerospace and Mechanical Engineering, The Graduate College, The University of Arizona, U.S.A., 2001.
9. Bhattacharjee P, Loth E. Simulations of laminar and transitional cold wall jets. *International Journal of Heat and Fluid Flow* 2004; **25**:32–43.
10. Sato H. The stability and transition of a two-dimensional jet. *Journal of Fluid Mechanics* 1960; **7**:53–80.
11. Sato H, Sakao F. An experimental investigation of the instability of a two-dimensional jet at low Reynolds numbers. *Journal of Fluid Mechanics* 1964; **20**:337–352.
12. Batchelor GK, Gill AE. Analysis of the stability of axisymmetric jets. *Journal of Fluid Mechanics* 1962; **14**:529–551.
13. Cohen J, Wygnanski I. The evolution instabilities in the axisymmetric jet. Part 1: the linear growth of disturbances near the nozzle. *Journal of Fluid Mechanics* 1987; **176**:191–219.
14. Sarma ASR, Sundararajan T, Ramjee V. Numerical simulation of confined laminar jet flows. *International Journal for Numerical Methods in Fluids* 2000; **33**:609–626.
15. Biswas G, Breuer M, Durst F. Backward-facing step flows for various expansion ratios at low and moderate Reynolds numbers. *Journal of Fluids Engineering* 2004; **126**:362–374.
16. Gu R. Modelling two-dimensional turbulent offset jets. *Journal of Hydraulic Engineering* 1996; **122**(11): 617–624.
17. Al-Sanea SA. Convection regimes and heat transfer characteristics along a continuously moving heated vertical plate. *International Journal of Heat and Fluid Flow* 2003; **24**:888–901.

18. Al-Sanea SA. Mixed convection heat transfer along a continuously moving heated vertical plate with suction or injection. *International Journal of Heat and Mass Transfer* 2004; **47**:1445–1465.
19. Roache PJ. *Fundamentals of Computational Fluid Dynamics*, Chapter 3. Hermosa, U.S.A., 1998.
20. Napolitano M, Pascazio G, Quartapelle L. A review of vorticity conditions in the numerical solution of the $\zeta - \psi$ equations. *Computers and Fluids* 1999; **28**:139–185.
21. Huang H, Wetton BR. Discrete compatibility in finite difference methods for viscous incompressible fluid flow. *Journal of Computational Physics* 1996; **126**:468–478.
22. Kang SH, Greif R. Flow and heat transfer to a circular cylinder with a hot impinging air jet. *International Journal of Heat and Mass Transfer* 1992; **35**(9):2173–2183.
23. Rao CG, Balaji C, Venkateshan SP. Conjugate mixed convection with surface radiation from a vertical plate with a discrete heat source. *Journal of Heat Transfer* 2001; **123**:698–702.
24. Kuyper RA, Van Der Meer ThH, Hoogendoorn CJ, Henkes RAWM. Numerical study of laminar and turbulent natural convection in an inclined square cavity. *International Journal of Heat and Mass Transfer* 1993; **36**(11):2899–2911.
25. Comini G, Manzan M, Nonino C. Finite element solution of the streamfunction-voriticity equations for incompressible two-dimensional flows. *International Journal for Numerical Methods in Fluids* 1994; **19**:513–525.
26. Ghia U, Ghia KN, Shin CT. High *Re* solutions for incompressible flow using the Navier–Stokes equations and multigrid method. *Journal of Computational Physics* 1982; **48**:387–411.
27. Armaly BF, Durst F, Pereira JCF, Schonung B. Experimental and theoretical investigation of backward-facing step flow. *Journal of Fluid Mechanics* 1983; **127**:473–496.
28. Gartling DK. A test problem for out flow boundary conditions flow over a backward-facing step. *International Journal for Numerical Methods in Fluids* 1990; **11**:953–967.
29. Durst F, Pereira JCF, Tropea C. The plane symmetric sudden expansion flow at low Reynolds numbers. *Journal of Fluid Mechanics* 1993; **248**:567–581.
30. Alleborn N, Nandakumar K, Raszillier H, Durst F. Further contributions on the two-dimensional flow in a sudden expansion. *Journal of Fluid Mechanics* 1997; **330**:169–188.
31. Battaglia F, Tavener SJ, Kulkarni AK, Merkle CL. Bifurcation of low Reynolds number flows in symmetric channels. 1997; **35**:99–105.
32. Amtec Engineering Inc. *TecPlot Version*: *9.0-0-9*, 2001.
33. Chiriac VA, Ortega A. A numerical study of the unsteady flow and heat transfer in a transitional confined slot jet impinging on an isothermal surface. *International Journal of Heat and Mass Transfer* 2002; **45**:1237–1248.

